Estimating surface solar irradiance from METEOSAT SEVIRI-derived cloud properties

H.M. Deneke [a,b,*], A.J. Feijt [a], R.A. Roebeling [a]

[a] Royal Netherlands Meteorological Institute, P.O. Box 201, 3730 AE De Bilt, Netherlands
[b] Meteorological Institute of the University of Bonn, Auf dem Hügel 21, 53111, Bonn, Germany

ARTICLE INFO

ABSTRACT

A satellite retrieval of surface solar irradiance based on METEOSAT SEVIRI-derived cloud properties is presented and validated for the Netherlands with one year of pyranometer measurements from 35 stations. The approach requires two independent steps: 1. Cloud properties are determined from narrow-band satellite radiances. 2. These cloud properties are used together with data on water vapor column and surface albedo to calculate the atmospheric flux transmittance. The retrieved irradiance is biased low by about 3–4 W/m^2 throughout the year, corresponding to an underestimate in atmospheric flux transmittance of about 0.015 in summer and 0.04 in winter. From a least-squares linear regression, residual standard deviations of 56 W/m^2 (0.072, 17.0%), 11 W/m^2 (0.052, 10.8%), and 4 W/m^2 (0.021, 4.2%) are found for hourly, daily and monthly mean irradiance (transmittance, relative error), respectively. These findings indicate that the accuracy of the retrieval is comparable to first-class pyranometers in the summer half year (5% of daily-mean values), but significantly lower in winter. Two aspects requiring further investigation have been identified: 1. For thin clouds, the atmospheric flux transmittance is strongly underestimated. 2. The retrieval accuracy is reduced for snow-covered surfaces.

1. Introduction

The sun is the primary source of energy for the earth's climate system and its five major components, the atmosphere, the biosphere, the cryosphere, the hydrosphere, and the land surface (IPCC, 2007). Hence, solar radiation is a key parameter for our understanding of the climate system, and the processes and interactions taking place within it.

A particularly important component of solar radiation is the surface solar irradiance (SSI), also commonly referred to as surface insolation, e.g. the amount of down-welling solar energy incident on a horizontal surface and integrated over the total solar spectrum. It governs the flux of solar energy at the interface between the atmosphere and the other components of the climate system, and thus determines the partitioning of solar energy between them.

The SSI is modulated by the atmospheric flux transmittance (AFT), which in turn depends on scattering and absorption by atmospheric gases, aerosols, and clouds. Clouds induce the largest changes, and have a high variability in space and time (Rossow & Lacis, 1990). Hence, accurate knowledge of cloud properties and cloud–radiation interactions are an important prerequisite for accurate estimates of the SSI.

Besides our scientific interest in the climate system, there is also a strong socioeconomic interest in spatially and temporally resolved information on SSI. To assess the potential of solar power plants, climatological information on SSI is essential (Robles Gil, 2007). For crop yield prediction and water resource management, the SSI allows to quantify evapotranspiration, plant growth, and soil moisture (Roebeling et al., 2004). Also, the forecasts of numerical weather prediction models can be improved by use of accurate fields of surface fluxes and soil moisture (van den Hurk et al., 1997).

To complement the sparse network of surface measurements, numerous algorithms have been developed to estimate the SSI from satellite radiances (see e.g. reviews by Pinker et al., 1995; Schmetz, 1989). However, the experimental nature of many algorithms in the fairly young field of satellite meteorology, the small number of overpasses of polar orbiting satellite systems, and the coarse spatial and spectral resolution of previous geostationary satellites has limited the adoption of satellite data in applications so far. The launch of the European METEOSAT-8 has changed this situation: satellite images of Europe and Africa are available at high spatial, spectral, and temporal resolution to continuously monitor the physical properties of clouds, and to quantify their influence on solar radiation.

The goal of the Surface Insolation in Cloudy Conditions from METEOSAT SEVIRI imagery (SICCS) project has been the extension and improvement of a retrieval previously developed at the Royal Netherlands Meteorological Institute (KNMI) for the estimation of the AFT and SSI from NOAA–AVHRR (Deneke et al., 2005), to be applicable to the METEOSAT Second Generation Spinning Enhanced Visible and Infrared Imager (MSG SEVIRI) instrument. The SICCS

* Corresponding author. Royal Netherlands Meteorological Institute, P.O. Box 201, 3730 AE De Bilt, Netherlands.
  E-mail address: deneke@knmi.nl (H.M. Deneke).

retrieval – the SSI retrieval developed during the project – does not directly use radiances as input. Instead, cloud properties from the cloud physical properties scheme (CPP, Roebeling et al., 2006), are used, which is being developed within EUMETSAT's Satellite Application Facility on Climate Monitoring (CM-SAF, see http://www.cmsaf.eu/). Both retrievals are based on lookup tables of detailed 1D radiative transfer calculations. Together, both algorithms provide a set of cloud properties and radiation components which are physically consistent within the framework of 1D radiative transfer theory. This model-based approach allows an easy extension of the algorithm to specific spectral regions (UV, photosynthetically active radiation) or to actinic fluxes.

However, there is also a drawback of this approach versus the more common choice of using empirical narrow-to-broadband conversion and angular distribution models for inferring the SSI. In particular, satellite-retrieved cloud properties are known to contain biases due to 3D radiative effects, which depend on the variability of clouds, and the sun and satellite geometries (Kato et al., 2006). Such effects are implicitly accounted for in empirical relations.

Thus, this study also contributes to the validation of the CPP retrieval, and enables the identification of cases when the model assumptions underlying the retrieval are not met. Ultimately, a reconciliation of both approaches seems desirable, by incorporating 3D radiative effects in both the inversion step of estimating cloud properties, and the forward model for predicting the SSI.

A necessary condition towards this goal is agreement between modeled and empirically determined behavior. As the principle provider of meteorological and climatological data for the Netherlands, KNMI's atmospheric research division has initiated the SICCS project to evaluate the benefits and drawbacks of satellite imager data in general, and the METEOSAT SEVIRI instrument in particular, for current applications relying on ground-based SSI measurements. To enable an objective evaluation, the retrieval accuracy is quantified for the Netherlands by comparison to a one year dataset of ground-based pyranometer measurements of global radiation from 35 meteorological stations.

A summary of required input data is given in Section 2, including the dataset used for validation. The retrieval algorithm is presented in Section 3. Section 4 presents the evaluation and some results of SICCS retrieval. A discussion is given in Section 5, followed by our conclusions and a brief outlook in Section 6.

2. Data

The SICCS retrieval relies on radiance data from the SEVIRI instrument as input. In addition, ancillary information on narrow-band surface albedo are required for the estimation of the cloud properties, on broadband surface albedo, and on the amount of precipitable water for the estimation of the SSI. The MOD43C2 surface albedo product based on the MODIS instrument, and the total precipitable water product generated by the CM-SAF are used for this purpose here. However, both products can easily be replaced by other datasets. An overview of SEVIRI is given first, followed by a description of the ancillary datasets. Finally, a summary of KNMI's pyranometer measurements is given, which are used for the evaluation of the SICCS retrieval.

2.1. METEOSAT-8 SEVIRI

METEOSAT Second Generation is a new series of European geostationary satellites operated by EUMETSAT. METEOSAT-8 is the first MSG satellite and has been launched in August 2002. It carries the SEVIRI and GERB instruments, and provides operational data since January 2004. It is positioned at 3.4°W over the equator. SEVIRI scans the complete disk of the earth 4 times per hour, and provides 12 spectral channels. These are 3 solar channels (0.6, 0.8 and 1.6 μm), 8

infrared channels (3.9, 6.2, 7.3, 8.7, 9.7, 10.8, 12.0 and 13.4 μm), and one high-resolution broadband visible channel (0.3–0.7 μm). The nadir spatial resolution of SEVIRI is 1×1 km^2 for the high-resolution channel, and 3×3 km^2 for all other channels.

2.2. Ancillary input data

The MOD43C surface albedo product is routinely derived from the MODIS instruments on NASA's Terra and Aqua satellites (Schaaf et al., 2002). All cloud-free observations during a 16-day period are aggregated on a 1×1 km^2 resolution sinusoidal equal area grid. If a sufficient number of cloud-free observations are available, the bi-directional reflectance distribution function (BRDF) is estimated for each gridbox. The black-sky albedo, defined as the albedo for a directed beam of radiation at the sun's elevation at local solar noon, and the white-sky albedo, which is applicable for completely isotropic down-welling radiation, are calculated from the BRDF. For the SICCS and CPP retrievals, only the white-sky albedo product is used, because clouds at moderate optical thickness attenuate the direct beam. Thus, most of the energy reaching the ground in cloudy conditions is contained in the diffuse irradiance. However, applying the black-sky albedo for the direct beam reflection has been verified to cause only minor differences even for thin clouds. The estimates of the broad-band visible (0.2–0.7 μm) and near-infrared (0.7–4.0 μm) albedo (Liang, 2001) are used for the SICCS retrieval, while the matching narrow-band channels are used by the CPP retrieval. To limit the amount of data, the 0.05° resolution product is used, which corresponds to a gridsize similar in magnitude to SEVIRI's pixel size.

The total precipitable water (TPW) product generated by the CM-SAF from the Advanced Television and Infrared Observation Satellite Operational Vertical Sounder (ATOVS) is used to account for changes in water vapor absorption. ATOVS is flown on NOAA's polar orbiting satellites and is composed of the AMSU-A and AMSU-B microwave radiometers, and the HIRS/3 infrared radiometer. These data have a resolution of 150×150 km^2. The retrieval algorithm uses an optimum estimation procedure to estimate the atmospheric temperature and humidity profiles (Reale, 2003). The CM-SAF TPW product provides a daily average for all satellite overpasses, and is regridded to 45×45 km^2 resolution.

Gaps in both data products are filled by temporal interpolation, and the data are reprojected to SEVIRI's geostationary satellite view projection (Wolf & Just, 1999) prior to their use in the local processing environment.

2.3. Pyranometer data for validation

KNMI maintains an operational network of 35 meteorological stations which measure the SSI alongside other meteorological parameters. Pyranometers of type *CM11* built by *Kipp en Zonen* are used. Pyranometers are thermoelectric instruments, which measure the differential heating of a black absorbing disc versus the shaded body of the instrument, and translate the temperature difference to the amount of radiation incident on the detector. A glass dome shields the instrument from environmental influences, but also limits the spectral sensitivity to 0.3–2.8 μm. The *CM11* instruments fulfill the accuracy requirements of a secondary standard pyranometer defined in ISO (1990) and WMO (1996), which are specified to be 3%. However, recent investigations suggest that the underlying estimates are likely too optimistic (Bush et al., 2000; Philipona, 2002).

Data loggers record the mean, minimum, and maximum level of irradiance measured by the instruments during 10-min intervals. As the instruments are operated without ventilation and heating, and are checked at rather long maintenance intervals of up to a year, the accuracy of the measurements is somewhat degraded by the deposition of pollution on the instrument's glass domes. Overall, the total error is not expected to exceed 5% (Kuik, 1997).

3. SICCS algorithm description

This section presents an overview of the SICCS retrieval for estimating the SSI, and the CPP retrieval which provides the cloud properties used as input data.

To calculate the SSI, denoted by the symbol F_{sfc}, both the irradiance F_{TOA} incident at the top-of-atmosphere (TOA), and the atmospheric flux transmittance T have to be known, which are linked by

$$F_{sfc} = F_0 \frac{\mu_0}{d^2} T. \tag{1}$$

Used are the solar constant F_0, with an assumed value of 1367 W/m², the cosine of the solar zenith angle μ_0 and the sun–earth distance d given in astronomical units. The sun position is calculated based on Michalsky (1988) and subsequent errata. Thus, the task of the SICCS retrieval is the estimation of the AFT for a given solar zenith angle, which is determined by the interaction of solar radiation with clouds, atmospheric aerosols and gases, and the surface.

3.1. The cloud physical properties retrieval

The CPP retrieval (Roebeling et al., 2006) has been developed at KNMI and is used operationally to provide climatological information on cloud phase, optical thickness, water path, and particle size from satellite imagers within the CM-SAF.

As a first step, cloudy pixels are identified. In KNMI's local processing, the CM-SAF cloud masking algorithm is replaced by a modified version of the cloud detection algorithm of the Moderate Resolution Imaging Spectroradiometer (MODIS) (Ackerman et al., 1998), which requires no ancillary input data such as surface temperature or atmospheric profiles and has been adapted to use SEVIRI radiances. It relies on spectral threshold and spatial coherence tests, and assigns one out of four confidence levels to a single pixel (clear certain, clear uncertain, cloud uncertain and cloudy certain). The source code can be found at http://www-loa.univ-lille1.fr/~riedi/soft/MSG_hrit2hdf_v1.4.tgz.

A clear atmosphere with zero cloud optical thickness is assumed for the probably clear and confident clear classes. For the cloudy certain and cloudy uncertain classes, cloud optical thickness and effective particle radius are retrieved simultaneously based on the method of Nakajima and King (1990). Cloud reflectances at a non-absorbing wavelength are dominated by cloud optical thickness (King, 1987), while reflectances at absorbing wavelengths are mainly a function of cloud particle size. The CPP retrieval algorithm uses SEVIRI's 1.6 and 0.6-μm channel for the absorbing and the non-absorbing wavelength, respectively.

The determination of cloud thermodynamic phase uses a consistency test of the observed difference in cloud reflectance at 0.6 and 1.6 μm, together with a threshold test in 11-μm brightness temperature. The consistency test compares the observed difference in cloud reflectance at 0.6 and 1.6 μm to modeled differences for ice and water clouds, which is a consequence of the stronger absorption of ice crystals at the 1.6-μm wavelength (Jolivet & Feijt, 2003).

Measured reflectances are compared to a lookup table of values obtained from the Doubling Adding KNMI (DAK, de Haan et al., 1987; Stammes, 2001) radiative transfer model (RTM). Calculations are performed using 80 Fourier terms for the azimuth and 180 Gaussian quadrature points for the zenith angle dependence. Radiances are stored at 65 different values of solar and viewing zenith angle (cosine from 1.0 to 0.2) and at 91 values of relative azimuth (0–180°). The lookup tables are generated using water and ice cloud profiles with 14 different values of cloud optical thickness (clear-sky, and 0.25–256 with exponentially increasing spacing). Mie calculations at 7 different effective radii determine the optical properties for the water clouds, while 4 sizes of imperfect hexagonal

crystals are used for ray-tracing calculations to characterize the ice clouds (Hess et al., 1998). The altitude of the water and ice cloud is fixed between 1–2 km and 8–9 km, respectively, and homogeneous profiles of cloud extinction are assumed. The atmosphere is modeled by the mid-latitude summer profile of Anderson et al. (1986), and gaseous absorption by ozone and NO_2 is taken into account explicitly. To account for other relevant absorbers, empirical line-to-band conversion factors are used, which have been derived from a comparison of collocated high-resolution SCIAMACHY spectra and SEVIRI radiances (Roebeling et al., 2006).

The RTM calculations are done first using a black surface. To account for the contribution by the surface albedo α_S, the measured bi-directional reflectance $r(\alpha_S)$ is calculated as (Chandrasekhar, 1950)

$$r(\alpha_S) = r_0 + \frac{\alpha_S T_0(\mu_0) T_0(\mu_V)}{1 - \alpha_S \alpha_A}, \tag{2}$$

which is exact for monochromatic radiation and Lambertian surfaces. Here, $T_0(\mu_0)$ and $T_0(\mu_V)$ are the AFT at the solar and viewing zenith angle above a black surface, r_0 the reflectance also above a black surface, and α_A is the hemispherical sky albedo for up-welling, isotropic radiation. The parameters $T(\mu)$ and α_A are obtained from two additional RTM calculations with differing, non-zero surface albedos, here chosen to be 0.5 and 1.0, to minimize numerical noise. Hence, Eq. (2) allows the calculation of the radiance above a gray surface for arbitrary values of the surface albedo. However, for non-Lambertian surface such as the ocean, significant errors may occur, in particular for thin clouds or clear-sky pixels close to the sun glint direction. These problematic cases can be excluded from further analysis based on quality flags provided by the cloud products.

At low sun elevations, the uncertainty in cloud property retrievals increases strongly, due to the increasing influence of 3D cloud effects (Kato et al., 2006) and due to the curvature of the earth. Therefore, the CPP algorithm is only applied for pixels with $\mu_0 > 0.2$.

3.2. The SICCS retrieval

The SICCS retrieval is an extension of the AVHRR surface solar irradiance retrieval presented by Deneke et al. (2005). In its current version, it takes into account variability induced by cloud properties, surface albedo and total precipitable water. Other sources of variability are neglected, for which climatological means are used. The conditions are matched to De Bilt (52.1° N, 5.2° E), and are considered to be representative for the Netherlands. The neglect of changes in aerosol properties is likely the largest source of error, in particular during clear skies, while other influences are expected to be minor (Deneke, 2002). Hence, some caution is advised if results are to be applied to different climate regimes, in particular with different aerosol properties. However, the assumed conditions can easily be adapted.

RTM calculations are done off-line with DISORT (Stamnes et al., 1988) using 16 streams and are stored in lookup tables. This code has been selected, as DAK in its current version does not include a band scheme for the broadband solar spectral region, and discrepancies between both numerical solvers have been found to be small for the SEVIRI spectral channels (Roebeling et al., 2005).

The cloud and atmospheric profiles and the grid of solar zenith angles used are identical to the ones for the CPP lookup table. Atmospheric gas absorption is parameterized by the 14 band correlated-k scheme of the rapid radiative transfer model (RRTM) (Mlawer & Clough, 1998), which includes water vapor, carbon dioxide, ozone, methane, and oxygen. Only a small sensitivity in column absorption is found for the well-mixed gases, ozone, as well as temperature and pressure (Deneke, 2002). However, typical changes in total precipitable water cause changes of up to 3% of TOA irradiance. A square root dependence following Li et al. (1993) is used to adjust

transmittances and reflectances from a reference value to the actual value of total precipitable water

$$T(\mathrm{pw}) = T_{\mathrm{ref}} + C\left(1 - \sqrt{\frac{\mathrm{pw}}{\mathrm{pw}_{\mathrm{ref}}}}\right),$$ (3)

where T denotes the AFT, pw the column amount of precipitable water, and $\mathrm{pw}_{\mathrm{ref}}$ the column amount of the reference profile. The climatological mean of 16.4 kg/m^2 (calculated from radiosondes launched at De Bilt, the Netherlands) is used as reference value, and a scale factor is used to adjust the water vapor profile. To determine C, two calculations are made using column values of 8.9 and 23.9 kg/m^2, which correspond to the mean value plus/minus one standard deviation (7.5 kg/m^2) of the radiosonde values. Eq. (3) is also applied to reflectances, and both to directional and hemispherical quantities.

An aerosol profile with an optical thickness of 0.19 at 0.55 μm of water-soluble composition is used. A log-normal distribution with modal radius of 70 nm and an effective variance of 1.7 is chosen. This treatment is consistent with the observations of Brink et al. (1997) and Stammes and Henzing (2000), as shown by Deneke (2002).

The RTM results for individual bands are aggregated into two spectral bands (0.2–0.7 and 0.7–4.5 μm). For both bands, the transmittance over a black surface T_0 and the constant C from Eq. (3) is found for each of the cloud profiles. The atmospheric back-scattering of surface-reflected radiation over a surface with albedo α_S is accounted for by

$$T(\alpha_S) = T_0 \frac{1}{1 - \alpha_S \alpha_A}.$$ (4)

Like in Eq. (2), the hemispherical sky albedo α_A for illumination from below is required.[1] Strictly, this equation only applies to monochromatic radiation, and is thus only used as an approximation. However, a sensitivity analysis has shown that resulting errors are small.

3.3. Estimation of daily-mean surface solar irradiance

Up to here, only instantaneous estimates of AFT and SSI have been discussed. For many applications, however, the SSI integrated over a specific time interval is of interest. In particular, cumulative sums of hourly, daily and monthly SSI are widely used. Strictly speaking, these sums quantify the deposited energy per unit area and should have SI units of J/m^2. For easier comparability, we nevertheless express numerical values as the average irradiance with units of W/m^2, which can be achieved by normalization with the length of the integration period.

The amount of irradiance incident at the TOA is proportional to the cosine of the solar zenith angle μ_0. Defining the temporal mean of the atmospheric flux transmittance $\bar{T}$ as the ratio of time-integrated irradiances at the TOA and surface, it is given as the weighted average of the instantaneous AFT using μ_0 as weighting factor:

$$\bar{T}(t_1, t_2) = \frac{\int_{t_1}^{t_2} \mu_0(t) T(t)\,\mathrm{d}t}{\int_{t_1}^{t_2} \mu_0(t)\,\mathrm{d}t}.$$ (5)

Thus, time averages of AFTs are calculated as μ_0-weighted mean, and not as arithmetic mean throughout this the paper for hourly, daily and monthly time averages of AFT.

As mentioned before, cloud property retrievals become unreliable at low sun elevations. Hence, the CPP scheme does not provide any data below $\mu_0 = 0.2$. Fig. 1 shows how different cut-off values for μ_0 affect the length of the daily retrieval period throughout the year, and the fraction of TOA irradiance captured by the retrieval during that
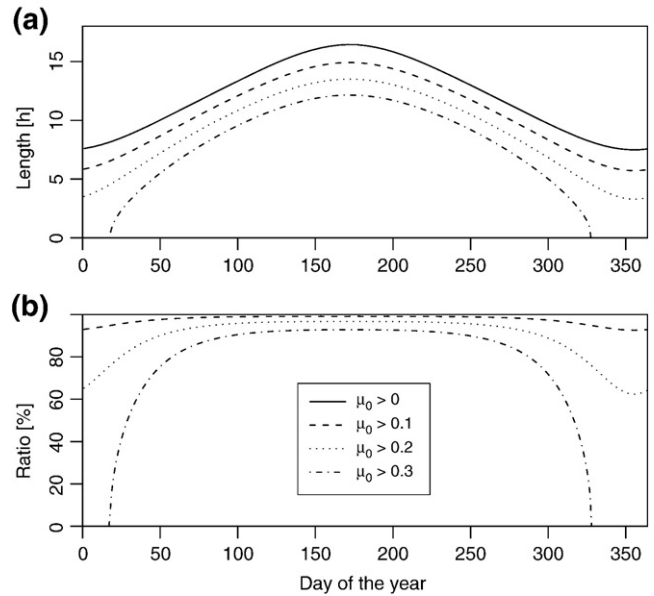
Fig. 1. Dependence of (a) period where sun exceeds different thresholds of the cosine of the solar zenith angle μ_0 (given in hours), and (b) ratio of TOA irradiance during the retrieval period to the total daily TOA irradiance (in percent) as a function of day of year. Data are valid for the location of Cabauw (51.97° N, 4.93° E).

time. These plots are valid for the station Cabauw (53.98° N, 4.93° E). For a cut-off value of 0.3, no retrievals are available during the months of December and January. At the cut-off value of 0.2 chosen for the CPP retrieval, 3 h of sunshine and about 10% of TOA irradiance are missed on average throughout the year. The missed fraction is largest in winter, reaching up to one third of total energy. This ratio will decrease further with latitude and limits the applicability of the retrieval for high-latitude regions during winter.

To still be able to estimate the daily-mean AFT and SSI, Eq. (5) is split into the sum of three partial transmittances,

$$\bar{T} = \frac{I_{\mathrm{TOA,M}}\tilde{T}_M + I_{\mathrm{TOA,MD}}T_{MD} + I_{\mathrm{TOA,E}}\tilde{T}_E}{I_{\mathrm{TOA,M}} + I_{\mathrm{TOA,MD}} + I_{\mathrm{TOA,E}}}.$$ (6)

The subscripts M, MD, and E denote the morning, midday, and evening periods, delimited by the moments of sunrise, sun exceeding and falling below $\mu_0 = 0.2$, and sunset. The values of TOA irradiance $I_{\mathrm{TOA,M}}$, $I_{\mathrm{TOA,MD}}$, and $I_{\mathrm{TOA,E}}$ are determined by numerical integration, and the time limits by numerical root finding of μ_0 as a function of time. Because the values of T_M and T_E are not known from the retrieval, estimates have to be used instead, as is indicated by the tilde in above formula. Multiplication by the total TOA irradiance will provide the cumulative daily SSI.

As the simplest possible choice, the average of all retrieved transmittances could be used to also estimate T_M and T_E. However, the AFT systematically decreases with μ_0 due to the increased atmospheric path-length. This is shown in Fig. 2 for the mean and percentile of AFT, which are plotted versus μ_0, based on surface measurements from the year 2004. Thus, this approach would systematically overestimate the daily-mean AFT and SSI. From the measurements, this overestimate would have a magnitude of 2.5 W/m^2 and 0.011 in SSI and transmittance.

Instead, we estimate T_M and T_E based on the two satellite-retrieved AFT values during the first/last 30-min periods after/before the sun zenith angle exceeds/falls below the value of $\mu_0 = 0.2$. A linear regression model based on pyranometer data from 2004 is used for this purpose. The following relation is obtained:

$$\tilde{T}_{M/E} = 0.682 T_{30\mathrm{min}} + 0.0309.$$ (7)
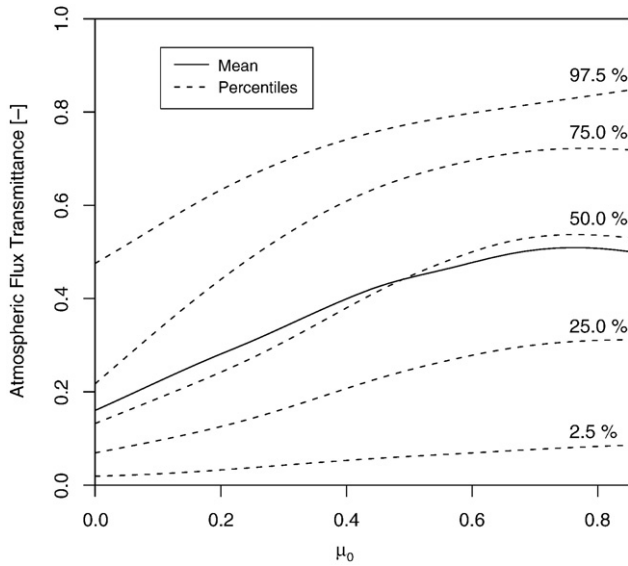
Fig. 2. Dependence of mean and percentile of atmospheric flux transmittance on the cosine of the solar zenith angle μ_0, as found from pyranometer measurements at 35 stations in the Netherlands for the year 2004.

A correlation of 0.83 is found between estimated and actual AFTs. Based on this model, the daily-mean AFT can be calculated with a standard deviation of 0.013 and a bias of 0.001 (corresponding to 1.3 and 0.1 W/m² in SSI).

To test the applicability of this empirical model to other time periods, it has been also applied to pyranometer data from 2006. Somewhat surprisingly, the performance of model is even slightly better than for the year 2004, with a reduction of standard deviation from 0.13 to 0.011 in AFT. Overall, these numbers show that the model is able to provide a bias-free and accurate correction for the missing retrievals at low sun elevations for the Netherlands. Prior to applications to other geographic regions, the model performance should be reevaluated with local measurements.

4. Results

In this section, the accuracy of the SICCS retrieval is evaluated by a comparison with pyranometer measurements, and some results of retrieval output are presented.

4.1. Evaluation with pyranometer measurements

Pyranometer measurements collected by KNMI at 35 stations in the Netherlands from June 2004 until May 2005 (see Section 2) are used to establish the accuracy of the SICCS retrieval. The evaluation is done for hourly, daily, and monthly averages of SSI, due to their common use in meteorological applications. Satellite-retrieved SSI products at 15-min resolution have been aggregated to match the corresponding averaging period. Retrieval results collocated above the ground stations are obtained from a grid of 2×4 satellite pixels. The spatial extent corresponds to an approximately square region of about 15×15 km². Assuming Taylor's frozen turbulence hypothesis, this region is slightly larger than the track length of a cloud due to the wind during SEVIRI's 15-min sampling time: Assuming a typical wind-speed of about 10 m/s², this corresponds to a track length of 9 km. Thus, this choice ensures a representative sampling of the cloud field passing over the pyranometer (Deneke et al., 2005).

Statistical parameters for this comparison are listed in Table 1 for both the SSI and the AFT. Results are also given separately for the summer and winter half year, as delimited by the times of the spring and autumn equinoxes, due to the notable difference in retrieval quality. While the SSI is mostly of interest for applications, the quality of the retrieval is better judged by the AFT, which removes the diurnal cycle of the TOA irradiance (see Eq. (1)).

Hourly and daily-mean values of surface solar irradiance and atmospheric transmission obtained by the SICCS retrieval are visualized in comparison to pyranometer measurements in Fig. 3.

The retrieved SSI shows a high correlation with the pyranometer measurements, with correlation coefficients of 0.965, 0.992, and 0.998 for hourly, daily and monthly mean SSI, respectively. For the atmospheric transmission, slightly lower correlations of 0.931, 0.955 and 0.977 are found. The statistics shown in Table 1 indicate that the quality of the retrieval is better in summer than in winter, both in terms of systematic bias and scatter. For the relative values of bias and scatter, this drop is amplified by the lower mean atmospheric transmission found in winter, which is due both to lower sun elevations and optically thicker clouds. An investigation of problematic cases has shown that the degradation is partly attributable to periods and regions with snow-covered surface. This is particularly evident for March 2005, which brought a short spell of cold weather and snow to the Netherlands. Considering this month alone, the correlation for daily-mean atmospheric transmission values drops to 0.73, which is significantly worse than the correlation for the complete winter half year.

Depending on the application, not only mean values of SSI are of interest, but also higher-order statistical moments or the distribution, and should therefore be preserved by the satellite retrieval. Fig. 4(a) shows percentiles of transmission as function of μ_0 for the pyranometer data and the retrieval. The mean change of AFT as a function of μ_0 for clear-sky, and for water clouds of optical thickness 1,4,16, and 64 has also been included as dotted lines. The change of retrieval quality with μ_0 is visualized in Fig. 4(b) by showing the percentiles of the error in atmospheric transmission.

The retrieval is found to accurately predict the atmospheric transmission for thick clouds. However, the AFT of thin clouds above values of about 0.4 is significantly underestimated. This value corresponds approximately to a water cloud with optical thickness of 4. The bias increases further with decreasing cloud optical thickness, reaching values up to about 0.1 for the 95th percentile. Two additional noteworthy features are visible: first, the μ_0 dependence of the AFT percentiles deviates significantly from that of the mean AFT at constant cloud optical thickness. Second, a significant number of cases are present where the pyranometer measurements exceed the clear-sky irradiance. Only a slight decrease of retrieval quality with decreasing sun elevation is observed in Fig. 4(b).

Table 1
Summary statistics of the evaluation of the SICCS retrieval with pyranometer data for (a) surface solar irradiance (in W/m²) and (b) atmospheric flux transmittance [unitless]

Period	Mean	Corr	Abs bias	Rel bias	Slope	Intercept	Abs sdev	Rel sdev
(a)								
Hourly	328.7	0.965	−13.9	−4.2	0.92	11.6	55.9	17.0
Daily	105.3	0.992	−3.7	−3.5	1.00	−3.2	11.4	10.8
Daily (summer)	193.1	0.977	−1.6	−0.8	0.93	10.8	12.8	6.6
Daily (winter)	39.9	0.946	−5.2	−13.1	0.87	−0.1	8.6	21.6
Monthly	116.5	0.998	−3.6	−3.0	1.02	−5.4	4.9	4.2
(b)								
Hourly	43.1	0.931	−0.020	−4.7	0.86	0.041	0.072	16.7
Daily	38.0	0.955	−0.029	−7.5	0.92	0.003	0.051	13.5
Daily (summer)	48.1	0.973	−0.014	−2.9	0.92	0.023	0.032	6.7
Daily (winter)	30.5	0.928	−0.039	−12.9	0.80	0.021	0.052	17.2
monthly	39.5	0.977	−0.026	−6.6	1.09	−0.062	0.021	5.4

Shown are the mean of the pyranometer data, the Pearson correlation coefficient (corr), the slope and intercept of a linear regression, and the residual standard deviation (sdev) between pyranometer data and retrieval. Both absolute (abs) and relative (rel, in %) values are listed for bias and standard deviation.
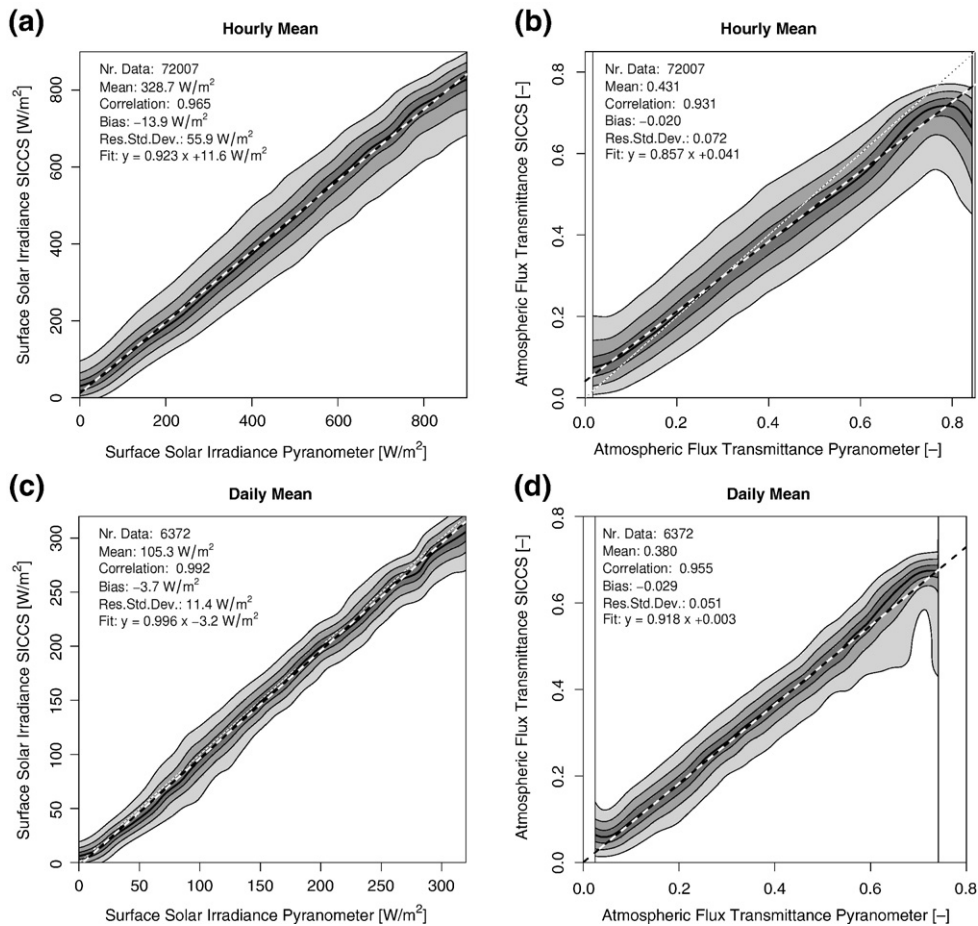
Fig. 3. Pyranometer measurements versus SICCS retrieval results for hourly (a, b) and daily (c, d) mean values of surface solar irradiance (a, c) and atmospheric transmission (b, d). For a given value of the pyranometer measurement, the shaded regions enclose 33, 66 and 95% of the SICCS retrieval results. The thick dashed lines show linear regression results obtained by considering both pyranometer and SICCS data as the dependent variable.

For clear-sky pixels, the estimate of SSI does not rely on the satellite reflectances, as the cloud optical thickness is fixed at zero. Thus, these cases can serve as independent test of the radiative transfer model and the representation of atmospheric state. To identify clear-sky situations, the satellite-based cloud detection is used, in combination with a threshold of 0.025 for the standard deviation in pyranometer-derived AFT to avoid cloud contamination. Results for the clear-sky cases are shown in Fig. 5. A small positive bias of 4.4 W/m^2, a standard deviation of 21.8 W/m^2, and a correlation of 0.987 are found. This indicates very good agreement of model and measurements. A dynamic adaption of aerosol properties based on instantaneous satellite radiances during clear-sky conditions could likely further reduce the standard deviation, and is a possible future improvement.

The findings summarized in the two previous paragraphs indicate that the treatment of the clear-sky atmospheric properties or deficiencies in the clear-sky RTM calculations cannot explain the observed retrieval bias for thin clouds. Instead, the bias has been found to increase with cloud cover (not shown), and is largest for completely overcast periods. Possible explanations for this behavior will be presented and discussed in Section 5.

Grouping all retrieved and measured values of daily-mean SSI by months, the boxplot shown in Fig. 6 is obtained. This type of plot is described in Tukey (1977). The gray-shaded boxes delimit the lower and upper quartile of retrieval and measurements for each month and dataset. The median is plotted as black bar, and the monthly means are shown by grey lines. The range from the 5th and 95th percentile maximum values is shown by the whiskers. A good agreement between retrieval and measurements throughout the year is clearly visible, as is the overall negative bias of the retrieval. As month with the lowest retrieval quality, March 2005 can be clearly identified, which is due to snow as has already been mentioned. This plot confirms visually that the SICCS retrieval is able to accurately reproduce the seasonal cycle of SSI both in terms of mean values and variability.

For June and December 2004, i.e. the months with highest and lowest sun elevation, and for March 2005, Fig. 7 shows the histogram of differences determined between daily-mean SSI from the SICCS retrieval and the pyranometer measurements. Due to the much higher level of mean irradiance, the histogram is significantly wider in June than in December. The large differences in March due to snow cover are also clearly visible.

4.2. Seasonal and annual averages of surface solar irradiance

In comparison to ground-based pyranometer measurements, the SICCS retrieval offers complete and highly resolved spatial coverage. This is clearly evident in Fig. 8, which shows results for central Europe including the Netherlands for the annual and seasonal SSI. Values are largest in summer and spring, and lowest in winter. This behavior is caused by the annual cycle of day length and sun elevation, and is further amplified by lower values of atmospheric transmissions observed in the winter half year.

Several interesting regional features can be identified. There is a large land–sea difference in the amount of SSI along the British channel during spring and summer. Throughout the year, rather low

(a)

(b)
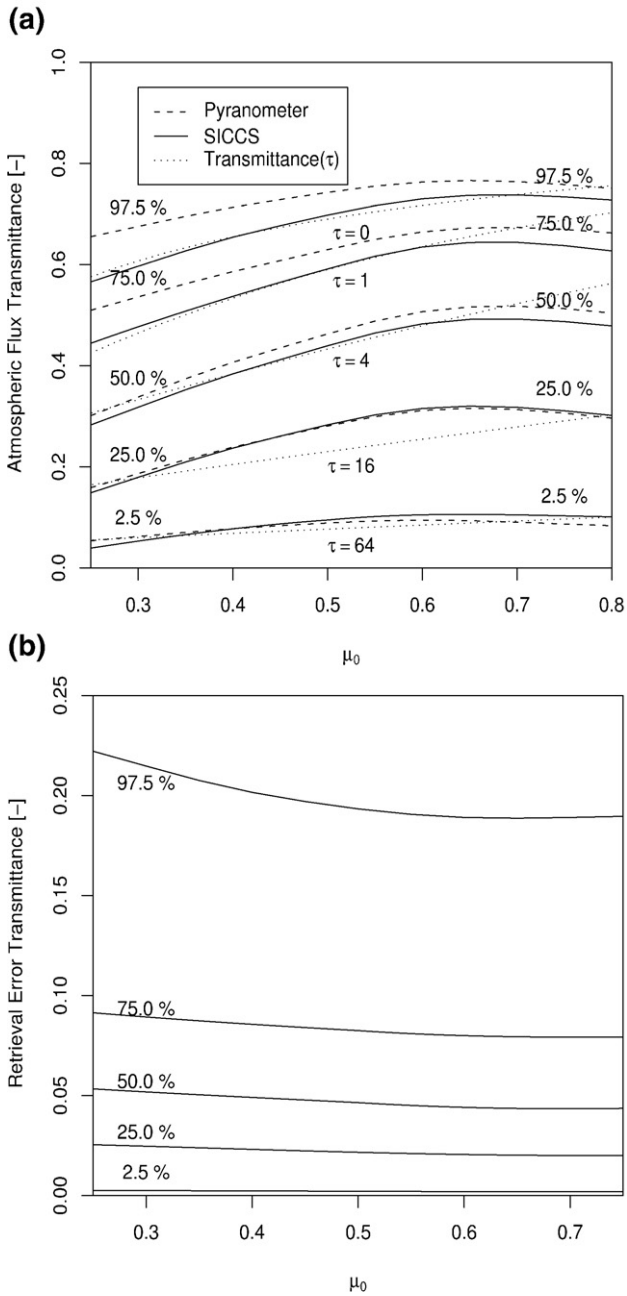
Fig. 4. (a) Percentiles of atmospheric flux transmittance for pyranometer data (dashed) and SICCS retrieval (solid) as function of μ_0. The mean modeled transmittance for water clouds at different values of optical thickness τ (see text) are also shown as dotted lines. (b) Percentiles of retrieval error in transmittance of the SICCS output as a function of μ_0.

values are found for central England. Strong orographic effects are evident along the Rhine rift valley along the French–German border in spring, with higher values observed along the valley versus the surrounding mountain ranges. To resolve similar features by a ground-based measurement network, an unrealistically high density of surface instruments would be required.

5. Discussion

The results and the current status of the retrieval are discussed in this section. First, the two shortcomings identified in the SICCS retrieval during the evaluation will be described, including proposed strategies for their rectification. Then, the overall retrieval accuracy will be put into perspective by a comparison with the accuracy of
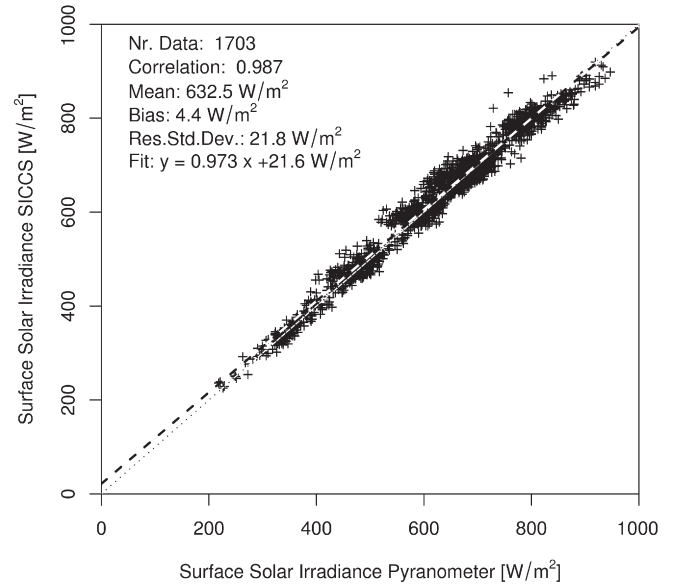
Fig. 5. Hourly mean values of surface solar irradiance predicted by SICCS retrieval versus pyranometer data for clear-sky cases.

ground-based measurements and three alternative MSG-based algorithms, and further relevant issues are mentioned.

The first shortcoming is the negative retrieval bias of about −0.02 in mean AFT, which has been attributed to thin clouds of optical thickness less than about 4, as is depicted in Fig. 4. Two factors contributing to this bias have been identified. First, the combination of MODIS surface albedo, and the optical properties of the clear-sky atmosphere contained in the CPP lookup tables, seem to underestimate the SEVIRI-observed clear-sky reflectance by about 0.01–0.03 on average. For clear-sky cases, this mismatch will not impact the SICCS algorithm, as the cloud optical thickness remains fixed to zero. Once a semi-transparent cloud is detected, the part of the observed reflectance that is not accounted for in the retrieval model will be erroneously attributed to the cloud. This causes an overestimate of cloud optical thickness, and an underestimate of cloud
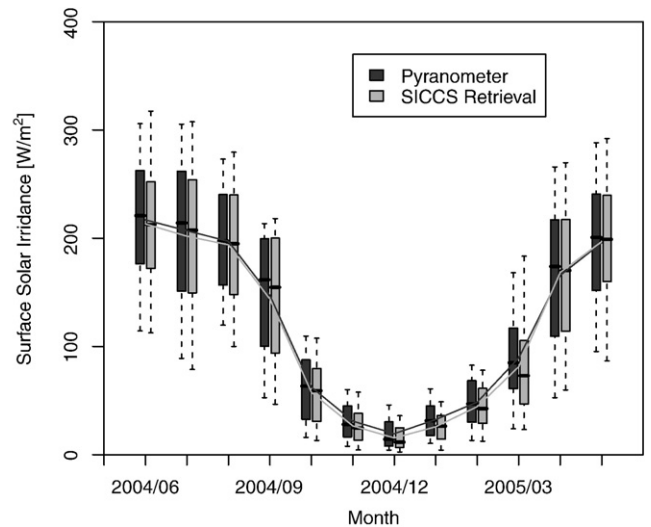
Fig. 6. Boxplot of daily-mean surface solar irradiance [in W/m²] from SICCS retrieval (light gray) and from pyranometer measurements (dark gray) and grouped by month. The boxes extend from the lower to the upper quartile, and the whiskers from the 2.5th to the 97.5th percentile. Monthly means are shown additionally as lines for both datasets.
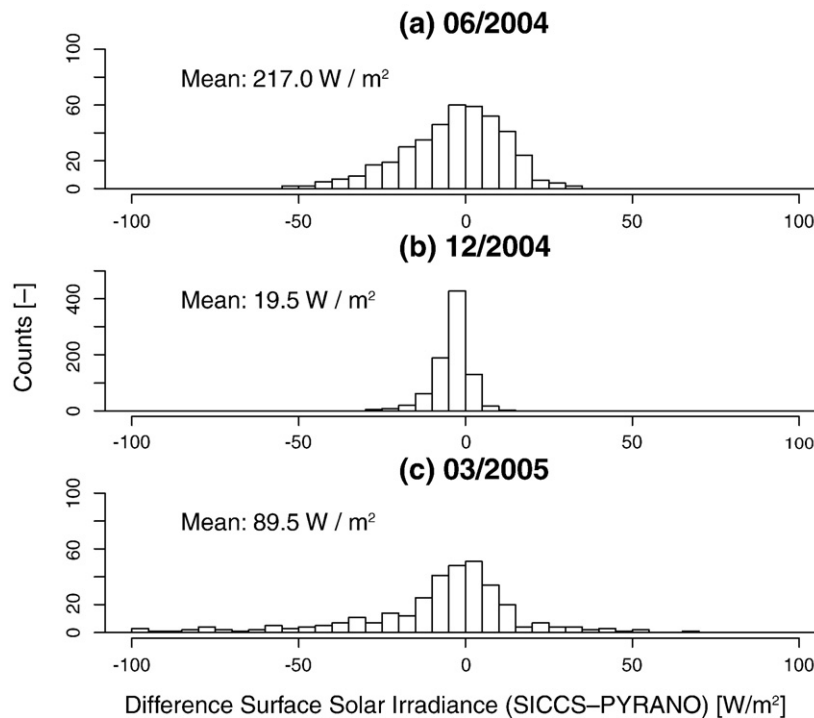
Fig. 7. Histogram of the difference in daily-mean surface solar irradiance (SICCS retrieval minus pyranometer measurements, in W/m^2) for (a) June 2004, (b) December 2004 and (c) March 2005. 5 W/m^2 is used as the bin size. The mean value found for the pyranometer measurements is also included.

transmittance. Possible explanations include bi-directional effects of the surface albedo, but also a low bias of MODIS versus SEVIRI clear-sky reflectances due to calibration differences. Such a bias would propagate to the MODIS inferred estimates of the surface albedo. The issue will be further investigated by generating and analyzing clear-sky composites of SEVIRI reflectances, and comparing them to MODIS scenes. Nevertheless, this effect is too small to fully explain the magnitude of the AFT bias. As a second factor, the neglect of 3D radiative effects and broken clouds by the CPP and SICCS retrievals is a potentially significant contribution to the AFT bias. Kato et al. (2006) show that biases between satellite-inferred and true cloud properties depend on both the sun and satellite viewing geometry, and propagate to radiative fluxes. Errors in the anisotropy of reflected radiation, which is largest for thin, homogeneous clouds, are identified as main reason. Based on MODIS scenes, Deneke et al. (2007) also conclude that about a quarter of all cloudy pixels at SEVIRI resolution are only partly cloud-filled, and cause large errors in retrieved cloud properties. The different solar zenith angle dependence of AFT percentiles and the transmittance at constant cloud optical thickness noted in Fig. 4(a) are possibly a hint for such biases. It could, however, be also explained by systematic changes in cloud optical thickness with solar zenith angle. The issues discussed here are highly relevant for the quality of the CPP-inferred cloud properties, and will be further investigated in the framework of KNMI's CM-SAF validation activities, as well as a EUMETSAT funded research fellowship.

As a second shortcoming, the presence of snow-covered surfaces significantly degrades the accuracy of the SICCS retrieval. Two mechanisms can be differentiated:

(1) The MODIS-retrieved surface reflectance is increased due to snow observed for some MODIS overpasses during a 16-day interval. If the snow has already melted at the time of a SEVIRI image, the SICCS retrieval will underestimate cloud optical thickness or even misclassify cloudy scenes as clear-sky. In consequence, the SSI is overestimated.

(2) High surface reflectances caused by short episodes of snow cover are not always resolved by the MODIS surface reflectance maps due to cloudiness. In those cases, the CPP retrieval overestimates cloud optical thickness, or leads to a misclassi-fication of snow-covered surfaces as clouds. Too little SSI is then predicted by the retrieval.

It is possible to partially address both effects by use of a snow-detection algorithm to differentiate cloudy from cloud-free pixels with snow cover (e.g. Gesell, 1989). However, rapid changes in surface albedo occur due to the falling and melting of snow, which cannot be monitored underneath clouds. Also, the accuracy of retrieved cloud properties is lower over bright surfaces, due to the reduction of contrast between cloudy and cloud-free radiances. Therefore, a reduced accuracy of the SICCS retrieval seems unavoidable for periods and regions with varying snow cover.

For applications requiring information about the SSI, pyranometer measurements are currently the most common data source. End users will therefore judge the accuracy of this and other satellite retrievals relative to the accuracy of these measurements. Typically, secondary standard or first-class pyranometers are used, with accuracy requirements specified in ISO (1990) and WMO (1996), and overall accuracies of 3% and 5%, respectively.

The errors of the retrieved atmospheric transmission have been quoted as fraction of the TOA irradiance so far. This choice has been made as errors can be compared independently of the value of mean atmospheric transmission, which depends on the local climate. Also, the magnitude of deviations seems to be nearly independent of the magnitude of atmospheric transmission. In contrast, pyranometer uncertainties are generally expressed relative to the current level of irradiance. Thus, the level of irradiance has to be known to compare both uncertainties.

For the daily SSI, the scatter observed between retrieval and pyranometer measurements is about 6–7% of the mean daily SSI in summer, and increases to over 20% in winter. Considering the uncertainties of the pyranometer measurements, and assuming
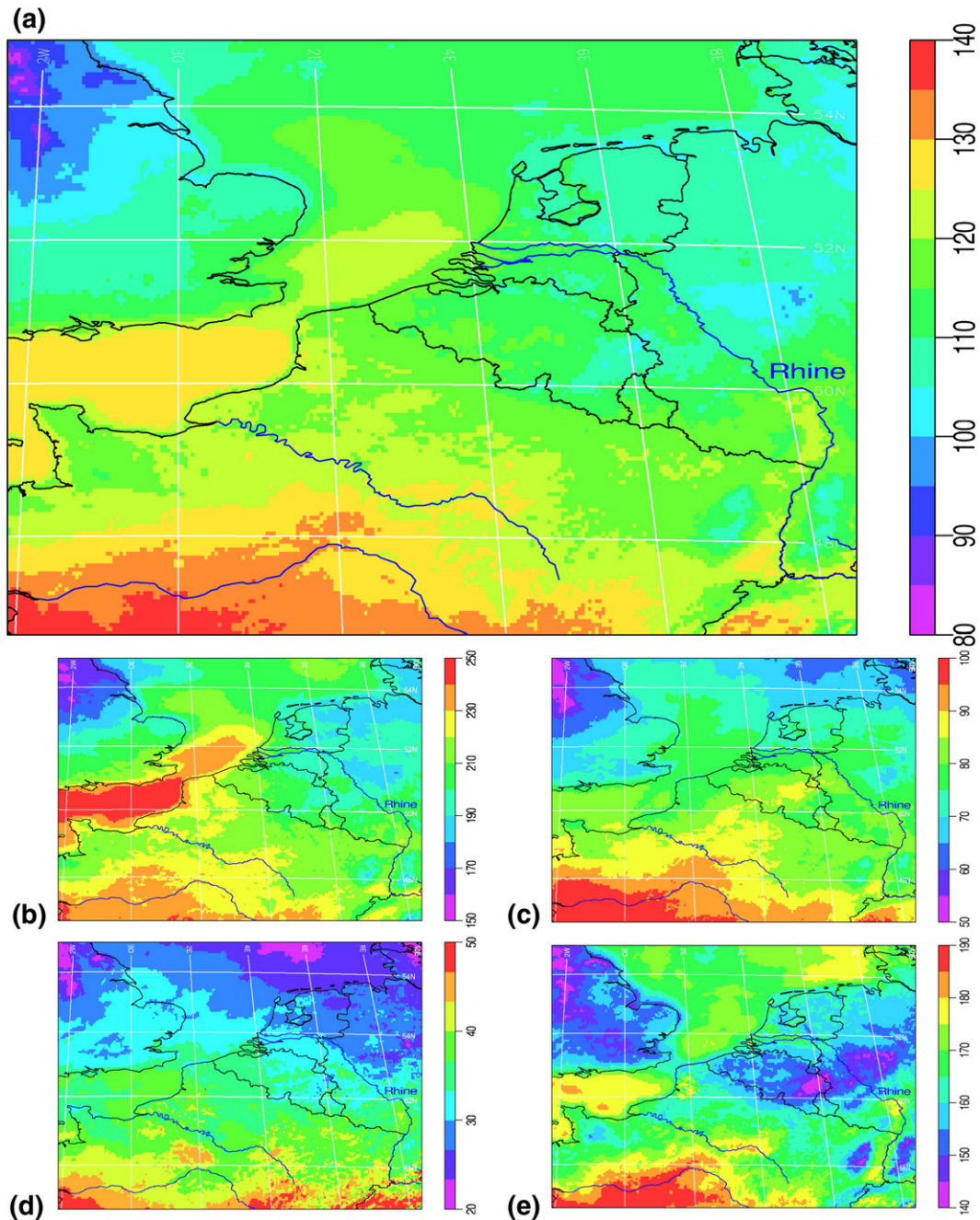
Fig. 8. Surface solar irradiance obtained by the SICCS retrieval [in W/m²]. Black and blue lines show country borders and rivers. (a) Annual average (June 2004–May 2005). Seasonal average for summer (b, June–August 2004), fall (c, September–November 2004), winter (d, December 2004–February 2005), and spring (e, March–May 2005), respectively. (For interpretation of the references to color in this figure legend, the reader is referred to the web version of this article.)

Gaussian error propagation, the SICCS retrieval is estimated to have an accuracy in the order of 5% or better in summer. This quality is comparable to measurements done with first-class pyranometers. In winter, however, the uncertainties are about 3–4 times as large as those of first-class pyranometers. While some part of this increase is attributable to the presence of snow as discussed above, the majority is in fact caused by the lower mean values of atmospheric transmission and the much smaller amount of TOA irradiance. Hence, an improvement to the level of accuracy of first-class pyranometers seems rather challenging.

Going from daily to hourly averages of SSI, the deviations between measurements and the SICCS retrieval increase to a mean annual value of about 15%. This increase can at least partly be attributed to sampling

effects. The retrieval provides an estimate of the SSI at SEVIRI's pixel resolution (about 4×7 km² for the Netherlands), while pyranometer records are nearly point measurements. This mismatch of sampling scales is known to introduce large scatter for sufficiently short averaging periods (Barker & Li, 1997; Deneke et al., 2005), in particular for broken cloud conditions. An example of such effects is visible in Fig. 3(b). Above a value of about 0.8 in AFT as determined by the pyranometer, the SICCS results drop of to lower values. Such cases often correspond to broken clouds, which enhance the local SSI above clear-sky levels, and are located within the satellite's field of view (see Deneke et al., 2005, for a more thorough discussion). No attempts to quantify such effects are made here. Still, end users should note that applications such as crop yield prediction and estimation of

evapotranspiration are mainly interested in the spatial average of SSI, so the smaller sampling scale of the pyranometer might actually be a disadvantage.

For potential users of satellite-retrieved SSI, the relative performance of different algorithms is of primary interest. Unfortunately, an objective inter-comparison of algorithms is a difficult task: several choices have to be made, and determine the precise numeric results: the location of surface stations, spatial and temporal averaging for satellite and surface data, the period of the evaluation, the comparison metrics, and possibly the sources for ancillary datasets (for the present algorithm, surface albedo and precipitable water). Towards this goal, the CM-SAF has initiated a visiting scientist activity to inter-compare SSI and other products from Meteosat SEVIRI generated by the Satellite Application Facilities on Climate Monitoring (CM), Ocean and Sea Ice (OSI), and Land Surface (LS) with surface measurements from 8 European stations (Ineichen, 2007). 10-min averages of SSI collected at 8 European stations from July and October 2005, and January and April 2006, have been compared to instantaneous satellite estimates obtained at each full hour. Here, the results obtained for the station of Cabauw are used as reference to quantify the accuracy of the SICCS algorithm, using results from July and October 2004, and January and April 2005. The SAF algorithms predict the SSI with standard deviations of 81 W/m^2 (OSI), 95 W/m^2 (LS), and 104 W/m^2 (CM), versus 98 W/m^2 for the SICCS algorithm. The SICCS algorithm shows the largest bias, underestimating the SSI by −11 W/m^2, versus biases of 1 W/m^2 (OSI), −7 W/m^2 (LS), and 5 W/m^2 (CM) for the SAF algorithms.

As a note of caution, the comparison at a single ground station, and using a different time period, has only limited significance: Ineichen (2007) also finds that bias and scatter of the satellite algorithms change significantly in between surface stations, and that changes can change the relative ranking of algorithms. Hence, the values presented here suggest that all algorithms exhibit scatter of similar order, but a more thorough comparison is required for any definite conclusions.

A further noteworthy point is the high sensitivity of the CPP retrieval to errors in sensor calibration (Feijt et al., 2004; Roebeling et al., 2006). Changes such as the unscheduled switch-over from METEOSAT-8 to METEOSAT-9 in September 2006 can potentially introduce large errors. Considerable efforts have been spent within the CM-SAF validation activities to inter-calibrate MODIS and METEOSAT-8 SEVIRI, and to compare satellite-derived cloud products to surface measurements (Roebeling et al., 2006). This task will be addressed by the *Global Space-based Inter-Calibration System* (GSICS) in the future, which has been initiated by the World Meteorological Organization (GSICS-IP, 2006).

6. Conclusions

This paper describes and evaluates the SICCS retrieval, which estimates the SSI and AFT from space using the METEOSAT SEVIRI-derived CM-SAF cloud property products. The retrieval is based on detailed radiative transfer calculations, and provides a set of cloud properties and shortwave radiative fluxes consistent within the framework of 1D radiative transfer, which does not rely on empirical parameterizations. A lack of reliable cloud retrievals at low sun elevations results in an incomplete sampling, and an overestimate of daily-mean atmospheric transmission. A linear model is used to correct for this bias.

The accuracy of the retrieval is quantified for the Netherlands by using one year of pyranometer measurements from 35 surface stations as reference. Throughout the year, the retrieved SSI is systematically underestimated by about 3–4 W/m^2. Due to the annual cycle of TOA irradiance, this value corresponds to a bias in atmospheric transmission of about 0.014 in summer, and 0.04 in winter. Residual standard deviations of 56 W/m^2 (0.072, 17.0%), 11 W/m^2 (0.052, 10.8%), and 4 W/m^2 (0.021, 4.2%) are found for hourly, daily, and monthly values of SSI (AFT, relative error) and individual station records.

Two aspects requiring improvement have been identified by the evaluation. First, the overall low bias in AFT can be attributed to cases with optically thin clouds (optical thickness smaller than about 4). Second, the accuracy of the retrieval is reduced for snow-covered regions. Strategies to address both issues have been outlined, and will be pursued in the near future.

The results presented in this paper confirm the high quality of the CM-SAF cloud properties obtained from SEVIRI, and show that they can be used to estimate the SSI with an accuracy comparable to first-class ground-based instruments in summer (5% for daily-mean values). In winter, the accuracy reduces significantly by a factor of about 3–4 due to the low elevation of the sun, the large satellite viewing angle for the Netherlands, and in some cases due to the presence of snow. In principle, the quality of the retrieval is expected to improve for lower latitudes, as these factors become less relevant. In particular, the accuracy for Africa and Southern Europe throughout the year is likely similar to that observed during summer for the Netherlands. Nevertheless, additional evaluation is required before applying this retrieval to other geographic regions: Kato et al. (2006) find that 3D radiative effects lead to significant biases in satellite-inferred radiative fluxes which depend on the viewing and sun geometry. This extension is planned for the future, and will also be of benefit for the validation of the CM-SAF cloud property products.

Considering the 15-min sampling time of METEOSAT SEVIRI, and the complete and highly resolved spatial coverage, output of the SICCS retrieval can serve as excellent source of information on SSI in addition to the traditional network of surface measurements. This holds in particular for regions with sparse data such as parts of Africa. Applications expected to benefit most include agriculture, water management, crop yield prediction, weather forecasting, climate research and the planning of solar power plants.

During the SICCS project, data streams have been set up to use MODIS-retrieved surface albedo and ATOVS estimates of total column water vapor as ancillary inputs. The retrieval is currently run in a pre-operational environment on demand for specific time periods. However, operational data processing by KNMI is currently being considered. Interested parties are encouraged to contact the authors for data availability or collaborations.

Acknowledgements

References

Ackerman, S. A., Strabala, K. I., Menzel, W. P., Frey, R. A., Moeller, C. C., & Gumley, L. E. (1998). Discriminating clear sky from clouds with MODIS. *Journal of Geophysical Research*, *103*, 32141–32157.

Anderson, G., Clough, S., Kneizys, F., & Chetwynd, J. (1986). AFGL atmospheric constituent profiles (0–120 km). *GL-TR-86-0110, Air Force Geophys. Lab., Hascom AFB, Mass., USA*.

Barker, H., & Li, Z. (1997). Interpreting shortwave albedo-transmittance plots: True or apparent anomalous absorption? *Geophysical Research Letters*, *24*, 2023–2027.

Brink, H. T., Kruisz, C., Kos, G., & Berner, A. (1997). Composition/size of the light-scattering aerosol in the Netherlands. *Atmospheric Environment*, *31*(23), 2502–2508.

Bush, B., Valero, F., Simpson, A., & Bignone, L. (2000). Characterization of thermal effects in pyranometers: A data correction algorithm for improved measurement of surface insolation. *Journal of Atmosphere and Ocean Technology*, *17*, 165–175.

Chandrasekhar, S. (1950). *Radiative transfer*. New York: Dover.

de Haan, J., Bosma, P., & Hovenier, J. (1987). The adding method for multiple scattering calculations of polarized light. *Astron. and Astrophys.*, *183*, 371–391.

Deneke, H., 2002. Influence of clouds on the solar radiation budget. Ph.D. thesis, University of Bonn, Bonn, Germany.

Deneke, H., Feijt, A., van Lammeren, A., & Simmer, C. (2005). Validation of a physical retrieval scheme of solar surface irradiances from narrow-band satellite radiances. *Journal of Applied Meteorology*, 44, 1453–1466.

Deneke, H., Roebeling, R., Wolters, E., & Feijt, A. (2007). Intercomparison of cloud properties retrieved from MSG SEVIRI and MODIS. *Proceedings of the Joint 2007 EUMETSAT and 15th AMS Conference*.

Feijt, A., Jolivet, D., Koelemeijer, R., Dlhopolsky, R., & Deneke, H. (2004). Recent improvements to LWP retrievals from AVHRR. *Atmospheric Research*, 72(2–4), 3–15.

Gesell, G. (1989). An algorithm for snow and ice detection using AVHRR data. An extension to the APOLLO software package. *International Journal of Remote Sensing*, 10(4–5), 897–905.

GSICS-IP. (2006). Implementation plan for a global space-based intercalibration system (GSICS). *Tech. rep., World Meteorological Organization* Switzerland: Geneva.

Hess, M., Koelemeijer, R., & Stammes, P. (1998). Scattering matrices of imperfect hexagonal ice crystals. *Journal of Quantitative Spectroscopy and Radiative Transfer*, 60, 301–308.

Ineichen, P. (2007). Satellite application facilities irradiance products: hourly time step comparison and validation. *Tech. rep.* Geneva, Italy: University of Geneva.

IPCC. (2007). Climate change 2007: The physical science basis. In S. Solomon, D. Qin, M. Manning, Z. Chen, M. Marquis, K. Averyt, M. Tignor, & H. Miller (Eds.), *Contribution of Working Group I to the Fourth Assessment Report of the Intergovernmental Panel on Climate Change* Cambridge, UK: Cambridge Univ. Press New York, USA.

ISO. (1990). Solar energy — Specification and classification of instruments for measuring hemispherical solar direct solar radiation. *ISO-TR 9060, International Organization for Standardization* Switzerland: Geneva.

Jolivet, D., & Feijt, A. (2003). Cloud thermodynamic phase and particle size estimation using the 0.67 and 1.6 micrometer channels from meteorological satellites. *Atmospheric Chemistry and Physics Discussions*.

Kato, S., Hinkelman, L., & Cheng, A. (2006). Estimate of satellite-derived cloud optical thickness and effective radius errors and their effect on computed domain-averaged irradiances. *Journal of Geophysical Research*, 111(D17), 17201–17217.

King, M. (1987). Determination of the scaled optical thickness of clouds from reflected solar radiation measurements. *Journal of the Atmospheric Sciences*, 44, 1734–1751.

Kuik, F. (1997). Global radiation measurements in the operational KNMI meteorological network — Effects of pollution and ventilation. *TR-197, Koninklijk Nederlands Meteorologisch Instituut* the Netherlands: De Bilt.

Li, Z., Leighton, H., Masuda, K., & Takashima, T. (1993). Estimation of SW flux absorbed at the surface from TOA reflected flux. *Journal of Climate*, 6, 317–330.

Liang, S. (2001). Narrowband to broadband conversion of land surface albedo. I. algorithms. *Remote Sensing of Environment*, 76.

Michalsky, J. (1988). The Astronomical Almanac's algorithm for approximate solar position (1950–2050). *Solar Energy*, 40, 227–235.

Mlawer, E., & Clough, S. (1998). Shortwave and longwave enhancements in the rapid radiative transfer model. *Proceedings of the 7th Atmospheric Radiation Measurement (ARM) Science Team Meeting*.

Nakajima, T., & King, M. (1990). Determination of the optical thickness and effective particle radius of clouds from reflected solar radiation measurements. Part I: Theory. *Journal of Atmospheric Sciences*, 47, 1878–1893.

Philipona, R. (2002). Underestimation of solar global and diffuse radiation measured at the Earth's surface. *Journal of Geophysical Research*, 107(D22), 4654.

Pinker, R., Frouin, R., & Li, Z. (1995). A review of satellite methods to derive surface shortwave irradiance. *Remote Sensing of Environment*, 51, 108–124.

Reale, A. (2003). NOAA operational sounding products for Advanced-TOVS. *ITSC XIII Proceedings* Canada: Sainte Adele.

Robles Gil, S. (2007). The socio-economic benefits of climatological services to the renewable energy sector. *WMO Bulletin*, 56(1), 40–45.

Roebeling, R., Berk, A., Frerichs, W., Jolivet, D., Stammes, P., Macke, A., et al. (2005). Sensitivity of cloud property retrievals to differences in narrow band radiative transfer simulations. *WR-2005-02, KNMI* the Netherlands: De Bilt.

Roebeling, R. A., Feijt, A. J., & Stammes, P. (2006). Cloud property retrievals for climate monitoring: implications of differences between SEVIRI on METEOSAT-8 and AVHRR on NOAA-17. *Journal of Geophysical Research*, 111, D20210. doi:10.1029/2005JD006990

Roebeling, R., van Putten, E., Genovese, G., & Rosema, A. (2004). Application of Meteosat derived meteorological information for crop yield predictions in Europe. *International Journal of Remote Sensing*, 25, 5389–5401.

Rossow, W., & Lacis, A. (1990). Global, seasonal cloud variations from satellite radiance measurements. part II: Cloud properties and radiative effects. *Journal of Climate*, 2, 419–462.

Schaaf, C., Gao, F., Strahler, A. H., Lucht, W., Li, X., Tsang, T., et al. (2002). First operational BRDF, albedo and nadir reflectance products from MODIS. *Remote Sensing of Environment*, 83.

Schmetz, J. (1989). Towards a surface radiation climatology: Retrieval of down-ward irradiances from satellites. *Atmospheric Research*, 23, 287–321.

Stammes, P. (2001). Spectral radiance modelling in the UV–visible range. *IRS 2000: Current problems in Atmospheric Radiation* (pp. 385–388).

Stammes, P., & Henzing, J. (2000). Multispectral aerosol optical thickness at De Bilt 1997–1999. *Journal of Aerosol Sciences*, 31, 283–284.

Stammes, K., Tsay, S., Wiscombe, W., & Jayaweera, K. (1988). Numerically stable algorithm for discrete-ordinate-method radiative transfer in multiple scattering and emitting layered media. *Applied Optics*, 27, 2502–2509.

Tukey, J. (1977). *Exploratory data analysis.* : Addison-Wesley.

van den Hurk, B., Bastiaanssen, W., Pelgrum, H., & van Meijgaard, E. (1997). A new methodology for initialization of soil moisture fields in numerical weather prediction models using METEOSAT and NOAA data. *Journal of Applied Meteorology*, 36, 1271–1283.

WMO. (1996). Guide to meteorological instruments and methods of observation. *WMO-No. 8, 6th edition* Geneva, Switzerland: World Meteorological Organization.

Wolf, R., & Just, D. (1999). LRIT/HRIT global specification. *CGMS 03, EU-METSAT, Darmstadt, Germany.*